Journal of Solid State Chemistry **156,** 75–83 (2001)
doi:10.1006/jssc.2000.8965, available online at http://www.idealibrary.com on IDEAL®

Single-Crystal X-Ray Diffraction Studies of Homologues in the Series $n\mathrm{Ba(Nb,Zr)O_3} + 3m\mathrm{NbO}$ with $n = 2, 3, 4, 5$ and $m = 1$

G. Nilsson* and G. Svensson†

*Departments of *Inorganic and †Structural Chemistry, Arrhenius Laboratory, Stockholm University, S-106 91 Stockholm, Sweden*

Received April 13, 2000; in revised form August 10, 2000; accepted September 15, 2000; published online December 21, 2000

Single crystals of four homologues in the series $n\mathrm{Ba(Nb,Zr)O_3} + 3m\mathrm{NbO}$, with $n{:}m = 2{:}1$, 3:1, 4:1, and 5:1, were found in the reduced Ba–Nb–Zr–O system. Single-crystal X-ray diffraction data were collected for all the crystals. For all homologues the space group was found to be *P4/mmm*. The structures can be described as intergrowths of $\mathrm{Ba(Nb,Zr)O_3}$ perovskite and NbO slabs. The refined cell parameters and compositions of the 2:1, 3:1, and 4:1 homologues are $a = 4.1768(5)$ Å and $c = 12.269(2)$ Å for $\mathrm{Ba_2Nb_{4.5(1)}Zr_{0.5(1)}O_9}$, $a = 4.1769(5)$ Å and $c = 16.493(3)$ Å for $\mathrm{Ba_{3+\delta}Nb_{4.8(2)-\delta}Zr_{1.2(2)}O_{12-\delta}}$ ($\delta = 0.098(4)$), and $a = 4.1747(6)$ Å and $c = 20.619(4)$ Å for $\mathrm{Ba_{4+\delta}Nb_{5.1(4)-\delta}Zr_{1.9(4)}O_{15-\delta}}$ ($\delta = 0.270(9)$). The refined cell parameters of the 5:1 homologue are $a = 4.1727(3)$ Å and $c = 24.804(3)$ Å. Zr replaces Nb only in the $\mathrm{NbO_6}$ octahedra found in the perovskite slabs. © 2001 Academic Press

INTRODUCTION

Investigations of the Ba–Nb–O, Sr–Nb–O, and K–Nb–O systems have, to date, resulted in a number of different intergrowth compounds (1, 2). Many of them consist of perovskite and $\mathrm{Nb_6O_{12}}$ units that are intergrown in multiple ways. The richness of these systems is a function of the crystallographic plane, {100} in the $\mathrm{Nb_6O_{12}}$ unit and {100} in the perovskite structure, across which these two structures can easily join (as indicated by dashed lines in Fig. 1), and the small difference in cell parameters (see below). Within these compounds the $\mathrm{Nb_6O_{12}}$ clusters are either found as discrete (3–5), condensed into dimers (6), formed as chains (7–9), formed as sheets (10, 11), or formed as an NbO network. The $\mathrm{Nb_6O_{12}}$ clusters consist of a central $\mathrm{Nb_6}$ octahedron, the edges of which are capped with oxygen atoms. These $\mathrm{Nb_6O_{12}}$ clusters can alternatively be seen as units of NbO. The structure of NbO is a defect rock-salt type with one-fourth of its cation and anion positions vacant (12). It can also be described as a three-dimensional condensation of $\mathrm{Nb_6O_{12}}$ via corner sharing of its central $\mathrm{Nb_6}$ octahedra (13). Besides the ordered intergrowths between perovskite and NbO, disordered intergrowths are very easily formed (14). The latter are often referred to as phasoids, as suggested by Magnéli (15).

The $\mathrm{Ba_2Nb_5O_9}$ structure belongs to the group of intergrowth compounds with 2D condensed $\mathrm{Nb_6O_{12}}$ clusters and is one homologue in the series $n\mathrm{ANbO_3} + 3m\mathrm{NbO}$ (A = Ba, K, Sr), n and m being the widths of the perovskite and NbO slabs, respectively. The structure can be described as an intergrowth of one NbO layer and two perovskite layers as shown in Fig. 2 ($m = 1$ and $n = 2$). In this series compounds with $m{:}n$ = 1:1, 2:1, 1:2, and 2:2 have also been reported (11, 16–18). The formal oxidation state of Nb ranges between +2 and +3 in the NbO layer and between +4 and +5 in the perovskite layer. The oxidation state of the Nb atom in the $\mathrm{NbO_6}$ octahedron in the latter is believed to play a vital role in stabilizing the structure with respect to the size mismatch between the NbO and perovskite regions (18).

Aliovalent substitution on the Nb site in the perovskite slabs is one way of affecting both the structure and the electrical properties. This was done in the $\mathrm{Ba_2Nb_{5-x}Ti_xO_9}$ ($0 \le x \le 1.0$) system, where a change in the electrical properties as a function of increasing amount of titanium was observed (19). However, titanium was found to replace Nb not only in the $\mathrm{NbO_6}$ octahedra but also in the NbO layers at sites that are five-coordinated by oxygen atoms. This is in agreement with the conditions found in TiO where Ti atoms are found with either $CN = 5$ or 6 (20, 21).

Another potential dopant for the $\mathrm{Ba_2Nb_5O_9}$ structure is Zr, a neighbor of Nb in the periodic system. The cubic $\mathrm{BaZrO_3}$ perovskite unit cell ($a = 4.181$ Å (22)) is closer in size to NbO ($a = 4.210$ Å (12, 23)) than is $\mathrm{BaNbO_3}$ ($a = 4.0884$ Å (24)). However, Zr is more reluctant to change its oxidation state from maximal (+4) than Nb is. This is reflected in the nonexistence of reduced barium zirconates as well as a compound with composition ZrO, and in the fact that no replacement of Nb by Zr in NbO has been reported (25). It is also well known that Zr has a preference for high coordination numbers to oxygen, ($CN = 6$, 7, 8); thus, Zr is seven-coordinated by oxygen in baddeleyite-type $\mathrm{ZrO_2}$ (26). It is therefore reasonable to expect Zr to enter the

0022-4596/01 $35.00

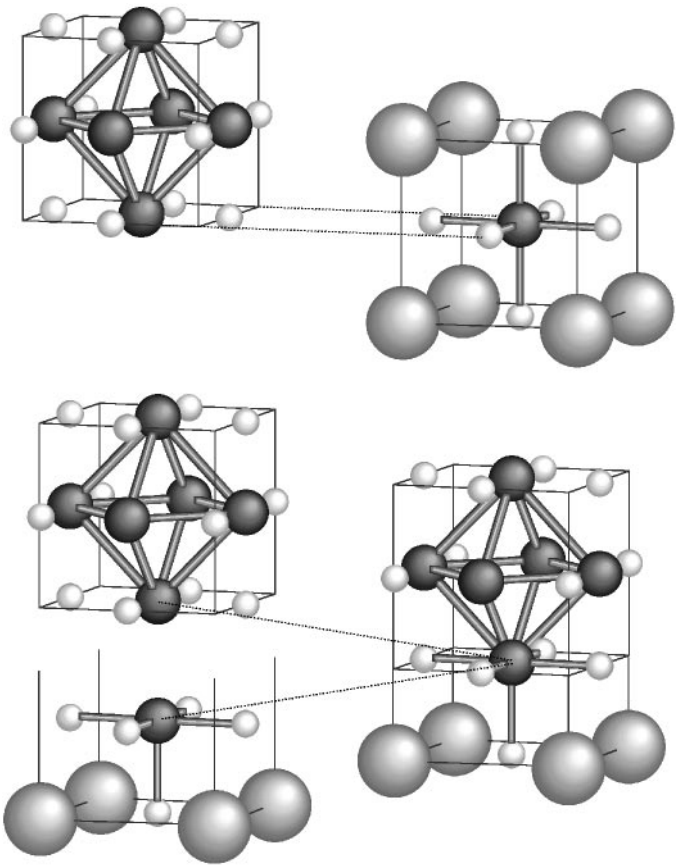

FIG. 1. Structure model of (a) the Nb_6O_{12} cluster (top left), (b) the perovskite structure (top right), and (c) a model showing the joining of one-half perovskite and one NbO unit (bottom).

MO_6 octahedra in intergrowth compounds of perovskite and NbO. The maximum Zr content expected in $Ba_2Nb_{5-x}Zr_xO_9$ would therefore be $x = 1$, when all NbO_6 octahedra have been replaced by ZrO_6 octahedra. In a study of the $Ba_2Nb_{5-x}Zr_xO_9$ system (27), no such compound was found. However, electron microscopy investigations and X-ray powder diffraction studies revealed the existence of new members in the series $nA\text{NbO}_3 + 3m\text{NbO}$. We will here report single-crystal X-ray diffraction investigations of these new homologues with $n = 2$, 3, 4, 5 and $m = 1$.

EXPERIMENTAL

Samples of $Ba_2Nb_{5-x}Zr_xO_9$ ($0 < x \leq 1.2$, in steps of 0.2, and $x = 1.5$), $Ba_2Nb_{4.5}Zr_{0.5}O_9$, $Ba_3Nb_5Zr_1O_{12}$, $Ba_4Nb_{5.5}Zr_{1.5}O_{15}$, $Ba_5Nb_6Zr_2O_{18}$, and $Ba_6Nb_{6.5}Zr_{2.5}O_{21}$ were prepared from pellets of stoichiometric mixtures of $BaCO_3$ (Merck p.a.), Nb_2O_5 (Roth, 99.9%), Nb (Aldrich, 99.8%), and ZrO_2 (Alfa, 99%), which had been thoroughly ground in an agate mortar, pressed to pellets sealed in niobium tubes under Ar, and then heated at 1600°C, 1625°C, or 1650°C for 10 h. A heating and cooling rate of $\sim$25°C/min was used.

The products were characterized by means of their X-ray powder diffraction patterns recorded in a Guinier–Hägg focusing camera, using Cu$K\alpha_1$ radiation ($\lambda = 1.54059$ Å) and powdered Si as internal standard. The films were evaluated with a scanner system (28).

A JEOL JSM820 scanning electron microscope (SEM), equipped with an energy-dispersive analyser (LINK AN10000), was used to determine the cation content of the single crystals. A ZAF correction was performed using the software provided by the manufacturer of the EDS equipment. Samples for transmission electron microscopy (TEM) studies were obtained by placing an ethanol suspension of crushed powder or selected single crystals on a holey carbon film supported by a copper grid. EDS analysis in the TEM was performed in a JEOL JEM2000FX equipped with a LINK 200QX at a high angle position. High-resolution electron microscopy (HREM) and electron diffraction studies were performed with a JEOL JEM3010 instrument, operated at 300 kV (side-entry sample holder, $\pm 20°$ xy-tilt).

Crystals suitable for single-crystal X-ray diffraction were picked from the samples under an optical microscope.

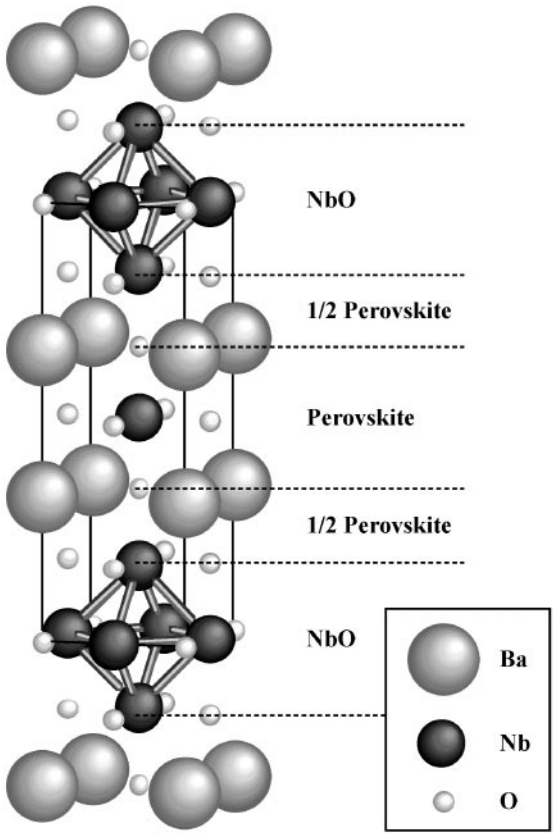

FIG. 2. Structure of $Ba_2Nb_5O_9$.

Single-crystal X-ray diffraction data were collected with a STOE image-plate diffractometer, using Mo$K\alpha_1$ radiation ($\lambda = 0.71073$ Å). The collected data were analyzed and integrated with the STOE program package (29). A numerical absorption correction was made with the Jana98 program (30), which was also used for structure refinement. The crystal shape was refined with the X-SHAPE program (29).

RESULTS AND DISCUSSION

All of the samples prepared were multiphasic according to powder X-ray diffraction patterns, with the exception of the samples prepared at $T = 1600$°C having $x = 0.2$ and $x = 0.4$ which were considered as close to single phase. Apart from some of the samples, which had melted, having a more metallic cluster, the samples were all black after heat treatment. Only a few samples yielded single crystals suitable for X-ray diffraction. Needle-like single crystals were selected from the sample prepared at 1600°C with $x = 0.2$, and plate-like crystals from the samples with $x = 1.5$ prepared at $T = 1600$°C and $T = 1625$°C. A more detailed phase analysis and HREM study is presented elsewhere (27). The samples prepared according to the stoichiometries $Ba_2Nb_{4.5}Zr_{0.5}O_9$, $Ba_3Nb_5Zr_1O_{12}$, $Ba_4Nb_{5.5}Zr_{1.5}O_{15}$, $Ba_5Nb_6Zr_2O_{18}$, and $Ba_6Nb_{6.5}Zr_{2.5}O_{21}$ yielded neither single-phase samples nor suitable single crystals.

Four different types of crystals were found, representing the homologues with n:m = 2:1, 3:1, 4:1, and 5:1. The crystals of 2:1 type, found in the sample with $x = 0.2$ heated at $T = 1600$°C, were often twinned. However, the ED and HREM studies in most cases showed them to be well ordered. The crystals of the 3:1 and 4:1 types found in samples with $x = 1.5$ heated at $T = 1625$°C, and that of the 5:1 type found in a sample with $x = 1.5$ heated at $T = 1600$°C, showed no evidence of twinning. To the contrary, extracted sections of reciprocal space (from raw data) exhibited streaking along a direction parallel to c*, indicating disorder. Three 1kl sections are shown in Fig. 3, representing the 3:1, 4:1, and 5:1 homologues, respectively. The 1kl section was chosen for presentation, because it best displays the streaking. By HREM imaging the disorder could be identified as stacking faults. Figure 4 shows a typical image of this phenomenon. However, occasionally rather well ordered crystals were found, as shown in Fig. 5. In the image only one defect is found, showing an NbO layer ending abruptly and being replaced by perovskite.

The presence of defects in the crystals makes it necessary to use a rather flexible definition of the term single crystal. Below we will use this term where distinct superstructure reflections are seen in projections of reciprocal space, neglecting streaking in between.

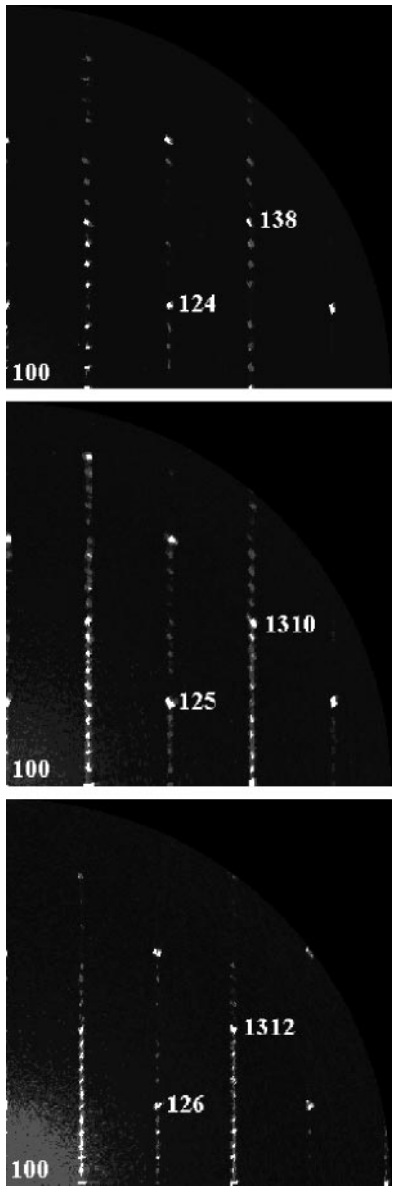

FIG. 3. Extracted sections of reciprocal space (from raw data) showing the 1kl section for the (from top to bottom) 3:1, 4:1, and 5:1 homologues.

3.1. Single-Crystal Structure Determination

The crystals used for the X-ray diffraction data collection were all analyzed in SEM by means of EDS. The cation content clearly distinguishes them as being four different homologues (see Table 1). These results were confirmed for the 2:1 and 3:1 homologues by SEM–EDS analysis of ~ 10 crystallites of each homologue (10–15 analyses on each) and TEM–EDS analysis of crystal fragments of the different homologues identified by ED, as shown in Tables 2 and 3, respectively. A structure model of each homologue as refined is presented in Fig. 6.

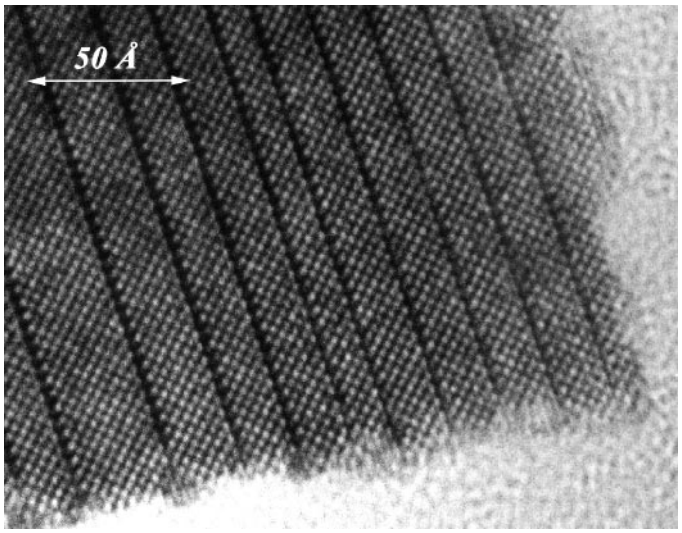

FIG. 4. HREM lattice image taken along the ⟨010⟩ direction, showing multiple stacking faults. The width of the perovskite slabs varies from 2 to 6 units. The image was recorded from a sample with the nominal composition $Ba_2Nb_{5-x}Zr_xO_9$ with $x = 1.5$, which had been heated at 1625°C.

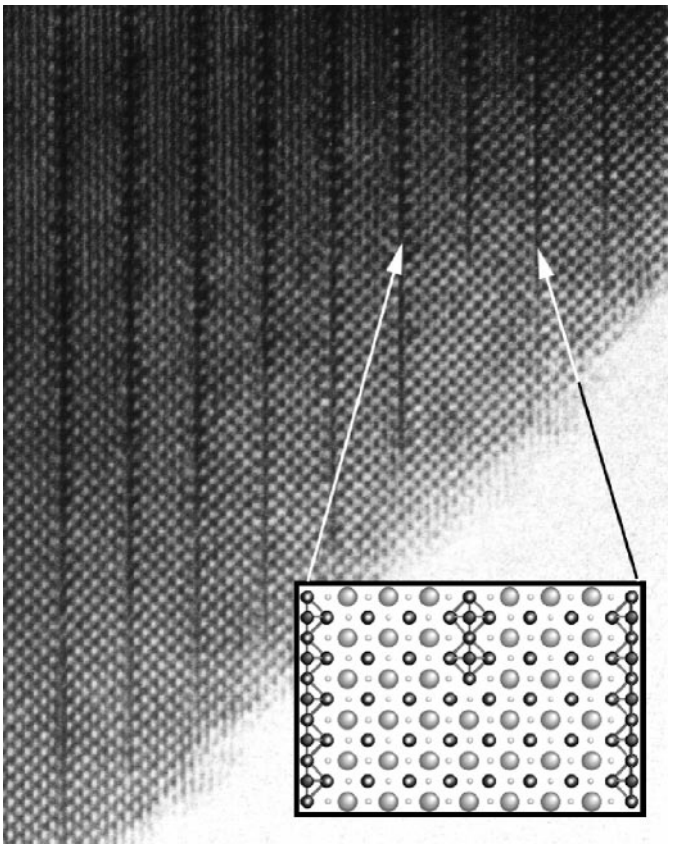

FIG. 5. HREM image taken along the ⟨010⟩ direction, showing a common type of defect. The NbO layer is ends abruptly and is replaced with perovskite, which doubles the c axis.

It was possible to index the data with a tetragonal unit cell in each of the different single-crystal X-ray diffraction studies (see below). For the 2:1 homologue, the cell parameters were found to be $a = 4.1768(5)$ Å and $c = 12.269(2)$, for the 3:1 homologue $a = 4.1769(5)$ Å and $c = 16.493(3)$ Å, for the 4:1 homologue $a = 4.1747(6)$ Å and $c = 20.619(4)$ Å, and for the 5:1 homologue $a = 4.1727(3)$ Å and $c = 24.804(3)$ Å. There were no systematically absent reflections in any of the collected data sets, which indicated the space group to be $P4/mmm$ for all homologues. This was expected and is consistent with the space group reported for other well-ordered compounds in the homologues series $nA\mathrm{NbO_3} + 3m\mathrm{NbO}$, such as $n{:}m = 1{:}1$ (A = Ba (11)), 2:1 (A = Sr (2), K (31), Ba (11), or Eu (32)), 1:2 (A = Ba (17)), and 2:2 (A = Sr(18)). A numerical absorption correction was applied, using the $4/mmm$ point group in each case.

$Ba_2Nb_{5-x}Zr_xO_9$. Inspection of reciprocal lattice of the crystallite selected for the X-ray diffraction study revealed no indications of disorder. The atomic coordinates of $Ba_2Nb_5O_9$ were used as a starting model. All thermal displacement parameters were refined isotropically, with the parameters for oxygen atoms constrained to be identical. Thermal anisotropy was tested for, but no significant evidence of such was found. The data were corrected for secondary extinction (type 1, isotropic, Gaussian (33)), because a small number of strong reflections yielded $F_o - F_c \ll 0$. Systematic testing of possible split Nb/Zr positions (Nb1, Nb2, and Nb3) showed that only position Nb3/Zr3 held any Zr, which was in agreement with expectations; see Introduction. The relative amount of Zr at the Nb3/Zr3 position was refined, keeping the atomic coordinates and thermal parameters identical. Although the refinement yielded no improvement of the R value, a split position is clearly indicated by the EDS analysis and was therefore used. The final refinement resulted in $R_{obs} = 0.0264$ and $R_{wobs} = 0.0273$. Detailed information on the data collection, refinement, atomic coordinates, and selected interatomic distances is given in Tables 4, 5, and 8. The refined composition, $Ba_2Nb_{4.6(1)}Zr_{0.4(1)}O_9$, is in good agreement with the cation content obtained by EDS analysis (see Table 1).

TABLE 1

Cation Content in the Different Homologues (Single Crystals) of the Series $nA\mathrm{NbO_3} + 3m\mathrm{NbO}$ with $n = 1$ and $m = 2$, 3, 4, and 5, as obtained by EDS Analysis in SEM Investigations

Homologue	Ba	Nb	Zr
$Ba_2Nb_{5-x}Zr_xO_9$	2.02(7)	4.56(7)	0.44(7)
$Ba_3Nb_{6-x}Zr_xO_{12}$	3.3(2)	4.5(2)	1.5(2)
$Ba_4Nb_{7-x}Zr_xO_{15}$	4.0(2)	4.5(4)	2.5(4)
$Ba_5Nb_{8-x}Zr_xO_{18}$	4.9(3)	6.4(1)	1.6(1)

TABLE 2

(a) SEM–EDS Analysis of $Ba_2Nb_{5-x}Zr_xO_9$ Type Crystallites in a Sample with $x = 0.4$ and (b) SEM–EDS Analysis of $Ba_3Nb_{6-x}Zr_xO_9$ Type Crystallites in a Sample with $x = 0.8$

(a)	
1600°C	$Ba_{1.98(2)}Nb_{4.70(7)}Zr_{0.30(7)}O_9$
1625°C	$Ba_{2.0(2)}Nb_{4.67(6)}Zr_{0.33(6)}O_9$
1650°C	$Ba_{2.3(2)}Nb_{4.55(7)}Zr_{0.45(7)}O_9$
(b)	
1600°C	$Ba_{3.0(2)}Nb_{5.0(2)}Zr_{1.0(2)}O_9$
1625°C	$Ba_{2.84(7)}Nb_{5.00(7)}Zr_{1.00(7)}O_9$
1650°C	$Ba_{2.8(2)}Nb_{5.1(2)}Zr_{0.9(2)}O_9$

TABLE 3

(a) TEM–EDS Analysis of $Ba_2Nb_{5-x}Zr_xO_9$ Type Crystallites and (b) TEM–EDS Analysis of $Ba_3Nb_{6-x}Zr_xO_9$ Type Crystallites in a Sample with $x = 0.8$

(a)	
1600°C	$Ba_{2.0(1)}Nb_{4.4(2)}Zr_{0.6(1)}O_9$
1625°C	$Ba_{2.0(2)}Nb_{4.6(3)}Zr_{0.4(2)}O_9$
1650°C	$Ba_{2.1(1)}Nb_{4.3(2)}Zr_{0.6(1)}O_9$
(b)	
1600°C	$Ba_{3.2(2)}Nb_{4.8(2)}Zr_{1.0(2)}O_9$
1625°C	$Ba_{3.0(1)}Nb_{4.6(2)}Zr_{1.4(2)}O_9$
1650°C	$Ba_{2.8(1)}Nb_{5.3(2)}Zr_{0.9(2)}O_9$

$Ba_3Nb_{6-x}Zr_xO_{12}$. The reciprocal lattice of the crystallite selected for the X-ray diffraction showed distinct superstructure reflections with some weak streaking in between. An idealized model of the $Ba_2Nb_5O_9$ structure, extended by one perovskite unit, was used as a starting point for the refinement. In the early stages, significant residual electron density was found at the O1 position. This effect is likely to stem from defects in the NbO layers, doubling the c-axis (in the same manner as seen in Fig. 5). The exchange of NbO for perovskite replaces the O1 atom with Ba, and at the same time also prohibits Nb1 from being present (considering metal–metal distances). The O1 position was therefore refined as a split position, shared with Ba (Ba4). The Ba4 occupancy parameter was in turn coupled to Nb1, reducing its occupancy parameter by an equal amount. The replacement of O1 by Ba4 is followed by an expected appearance of an extra oxygen atom at ($\frac{1}{2}$, $\frac{1}{2}$, 0). However, inserting an O atom at this position resulted in all oxygen atoms having negative temperature displacement parameters. Considering that the electron density of this extra oxygen is of the same magnitude as the average residual electron density, it was decided not to invoke this change. As an additional result of the disorder, it was also found that the substructure reflections of type hkl with $l = 4n$ had to be separately scaled. The reason for this is that while the intensity of superstructure reflections from the $n = 3$, $m = 1$ homologue mainly stems from this phase, the sublattice reflections are common for all homologues, irrespective of the amount of disorder. The effect is expected as an increased level of disorder in the end will result in only substructure

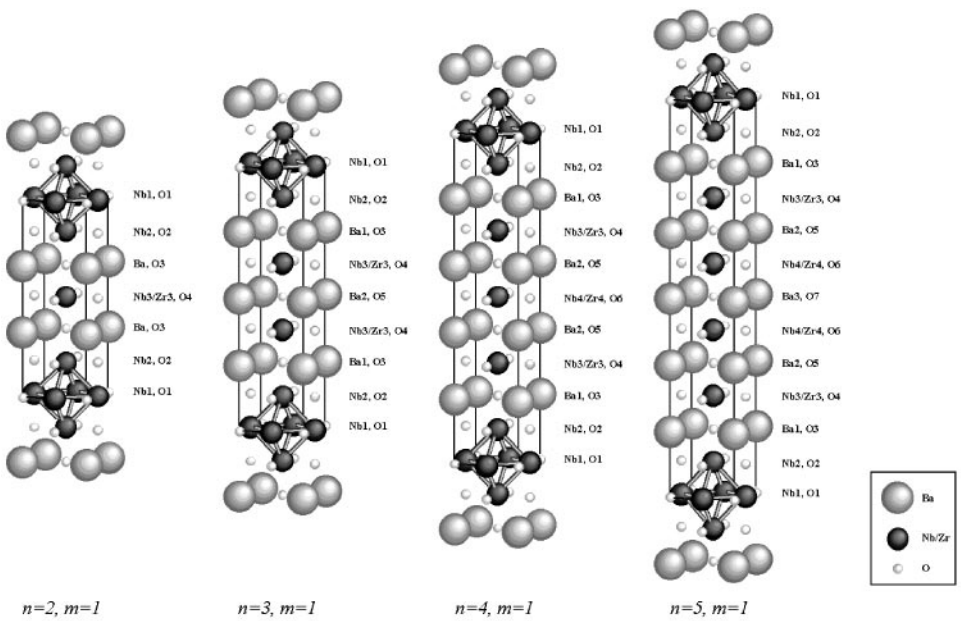

FIG. 6. Structure models of the different homologues in the series nBa(Nb, Zr)O_3 + 3mNbO with n:m = 2:1, 3:1, 4:1, and 5:1. In the structure model of n:m = 5:1 all atoms are at idealized positions. The other models are based on the coordinates obtained in the structure refinements.

TABLE 4
Crystal Data and Experimental Conditions for the Structure Determination of (A) $Ba_2Nb_{4.5(1)}Zr_{0.5(1)}O_9$, (B) $Ba_{3+\delta}Nb_{4.8(2)-\delta}Zr_{1.2(2)}O_{12-\delta}$, and (C) $Ba_{4+\delta}Nb_{5.1(4)-\delta}Zr_{15-\delta}O_{15-\delta}$

	(A)	(B)	(C)
Formula weight (g/mol)	882.4	1159.4	1436.5
Symmetry	Tetragonal	Tetragonal	Tetragonal
Space group (No.), Z	$P4/mmm$(123), 1	$P4/mmm$(123), 1	$P4/mmm$(123), 1
Lattice parameters (Å)			
a	4.1768(5)	4.1769(5)	4.1747(6)
c	12.269(2)	16.493(3)	20.619(4)
Volume (Å^3)	214.05(5)	287.74(7)	359.4(1)
Density calcd. (g/cm^3)			
($\delta = 0$)	6.845	6.691	6.638
Diffractometer	Stoe IPDS	Stoe IPDS	Stoe IPDS
IP distance (mm)	80	80	80
Radiation (Å)	Mo$K\alpha$ ($\lambda = 0.71073$)	Mo$K\alpha$ ($\lambda = 0.71073$)	Mo$K\alpha$ ($\lambda = 0.71073$)
Temperature (K)	298	298	298
Crystal shape	Needle	Plate	Plate
Data collection mode	φ-Scan	φ-Scan	φ-Scan
Range of hkl			
h	$-4 \rightarrow 4$	$-4 \rightarrow 4$	$-4 \rightarrow 4$
k	$-4 \rightarrow 4$	$-4 \rightarrow 4$	$-4 \rightarrow 4$
l	$-13 \rightarrow 14$	$-18 \rightarrow 18$	$-23 \rightarrow 23$
Reflections	1152	1848	2257
Unique reflections	140	183	220
Observed reflections	130	166	155
Criterion for significance	$I_{obs} > 3\sigma(I_{obs})$	$I_{obs} > 3\sigma(I_{obs})$	$I_{obs} > 3\sigma(I_{obs})$
R_{int} (obs; all)	7.49; 7.98	5.00; 5.03	3.88; 4.09
Absorption correction	Numerical	Numerical	Numerical
μ (mm^{-1})	15.4697	16.3619	15.8789
T_{min}	0.3481	0.3461	0.4360
T_{max}	0.8879	0.6883	0.9193
Method of refinement	F	F	F
Parameters refined	12	16	20
R(obs)	0.0264	0.0335	0.0311
R_w(obs)	0.0273	0.0337	0.0317
R(all)	0.0320	0.0385	0.0421
R_w(all)	0.0279	0.0339	0.0319
Goof (all; obs)	1.91; 1.87	3.88; 3.70	2.95; 2.44
Weghting scheme	$w = 1/\sigma^2(F_o)$	$w = 1/\sigma^2(F_o)$	$w = 1/\sigma^2(F_o)$
$(\Delta/\sigma)_{max}$	0.0007	0.0014	0.0003
$\Delta\rho_{min};\Delta\rho_{max}$ (e$^-$/Å^3)	$-2,39$; 1.57	-3.05; 2.50	-1.63; 3.04
Ext. coeff. (type 1, Gaussian, isotr.)	0.02(1)	None	None

reflections, thus showing mainly perovskite/NbO reflections. The latter yielded a significant improvement in the refinement. The anisotropy of the thermal displacement parameters for the different metal atom position was tested, but no significant indications were found, and isotropic parameters were therefore used. The O and Ba4 atoms were all refined with identical thermal displacement parameters. The final refinement cycle yielded $R_{obs} = 3.35\%$ and $R_{wobs} = 3.37\%$. Corresponding structural data, fractional coordinates, and selected interatomic distances are displayed in Tables 4, 6, and 8. The refined composition, $Ba_{3+\delta}Nb_{4.8(2)-\delta}Zr_{1.2(2)}O_{12-\delta}$ ($\delta = 0.140(3)$), agrees with the cation content found by EDS analysis (see Table 1).

TABLE 5
Fractional Coordinates, Occupational Parameters, and Isotropic Thermal Displacement Parameters for $Ba_2Nb_{4.5(1)}Zr_{0.5(1)}O_9$

Atom	Mult.	Occ.	x	y	z	U_{iso}
Ba	8	1	0	0	0.33122(4)	0.0055(3)
Nb1	8	1	0.5	0	0	0.0021(4)
Nb2	8	1	0.5	0.5	0.16311(6)	0.0015(3)
Nb3	16	0.5(1)	0.5	0.5	0.5	0.0012(6)
Zr3	16	0.5(1)	0.5	0.5	0.5	0.0012(6)
O1	16	1	0	0	0	0.0046(8)
O2	4	1	0.5	0	0.1730(3)	0.0046(8)
O3	8	1	0.5	0.5	0.3394(5)	0.0046(8)
O4	8	1	0.5	0	0.5	0.0046(8)

$Ba_4Nb_{7-x}Zr_xO_{15}$. The extracted sections of reciprocal space showed quadruple superstructure reflections, consistent with the 4:1 homologue, with a small streaking in between indicating an increased degree of disorder (see Fig. 3). A model of the $Ba_2Nb_5O_9$ structure, with the perovskite layer widened by two units and all atoms in ideal positions, constituted the starting model. Calculating the difference electron density revealed the same type of disorder found in the case of the 3:1 homologue. The O1 position was therefore assumed to be split in the same way as for the 3:1 homologue discussed above. Moreover, a scaling of reflections similar to that for the 3:1 homologue above was used, scaling reflections of type hkl with $l = 5n$ and $h + k + l = 2n$ separately. All atoms were refined with isotropic thermal displacement parameters, keeping the thermal parameters for O atoms and Ba4 identical. Thermal displacement parameters for the metal atoms were all checked for anisotropy, but there were no significant indications of such. Assuming Nb3 and Nb4 to be split Nb/Zr positions, using the arguments in the Introduction, resulted in a significant improve-

TABLE 6
Fractional Coordinates, Occupational Parameters, and Isotropic Thermal Displacement Parameters for $Ba_{3+\delta}Nb_{4.8(2)-\delta}Zr_{1.2(2)}O_{12-\delta}$

Atom	Mult.	Occ.	x	y	z	U_{iso}
Ba1	8	1	0	0	0.24652(3)	0.0049(2)
Ba2	16	1	0	0	0.5	0.0056(2)
Nb1	8	0.860(3)	0.5	0	0	0.0021(3)
Nb2	8	1	0.5	0.5	0.12172(5)	0.0036(2)
Nb3	8	0.42(8)	0.5	0.5	0.37360(4)	0.0033(4)
Zr3	8	0.58(8)	0.5	0.5	0.37360(4)	0.0033(4)
O1	16	0.860(3)	0	0	0	0.0008(7)
Ba4	16	0.140(3)	0	0	0	0.0008(7)
O2	4	1	0.5	0	0.1273(2)	0.0008(7)
O3	8	1	0.5	0.5	0.2522(3)	0.0008(7)
O4	8	1	0.5	0	0.3760(2)	0.0008(7)
O5	16	1	0.5	0.5	0.5	0.0008(7)

TABLE 7
Fractional Coordinates, Occupational Parameters, and Isotropic Thermal Displacement Parameters for $Ba_{4+\delta}Nb_{5.1(4)-\delta}Zr_{1.9(4)}O_{15-\delta}$

Atom	Mult.	Occ.	x	y	z	U_{iso}
Ba1	8	1	0	0	0.19714(5)	0.0060(3)
Ba2	8	1	0	0	0.39915(5)	0.0057(3)
Nb1	8	0.746(9)	0.5	0	0	0.0031(6)
Nb2	8	1	0.5	0.5	0.09762(9)	0.0024(4)
Nb3	8	0.4(1)	0.5	0.5	0.29857(8)	0.0014(6)
Zr3	8	0.6(1)	0.5	0.5	0.29857(8)	0.0014(6)
Nb4	16	0.3(2)	0.5	0.5	0.5	0.0025(9)
Zr4	16	0.7(2)	0.5	0.5	0.5	0.0025(9)
O1	16	0.746(9)	0	0	0	0.0043(8)
Ba4	16	0.254(9)	0	0	0	0.0043(8)
O2	4	1	0.5	0	0.1031(4)	0.0043(8)
O3	8	1	0.5	0.5	0.2011(5)	0.0043(8)
O4	4	1	0.5	0	0.3006(3)	0.0043(8)
O5	8	1	0.5	0.5	0.3994(5)	0.0043(8)
O6	8	1	0	0.5	0.5	0.0043(8)

ment of the R value, from 4.65% down to 3.11%. The final refinement yielded $R_{obs} = 3.11\%$ and $R_{wobs} = 3.17\%$. Corresponding structural data, fractional coordinates, and selected interatomic distances are presented in Tables 4, 7, and 8. The refined composition $Ba_{4+\delta}Nb_{5.1(4)-\delta}Zr_{1.9(4)}O_{15-\delta}$ ($\delta = 0.254(9)$) agrees with the cation content found by EDS analysis (see Table 1).

$Ba_5Nb_{8-x}Zr_xO_{18}$. The X-ray diffraction data collected for a crystal of the 5:1 homologue exhibited quintupling of superstructure reflections overlaid by severe streaking. Due to the high degree of disorder it was not possible to use these data for structure refinement. Using an ideal model of $Ba_2Nb_5O_9$, with the width of the perovskite layer extended by three units as shown in Fig. 6 ($n = 5, m = 1$), did however indicate that the structure is essentially as expected. In the extracted section of reciprocal space (see Fig. 3) the increased level of disorder can, besides streaking, be seen as generally weaker superstructure reflections. The effect is expected, as an increased level of disorder in the end will result in only substructure reflections, thus showing mainly perovskite/NbO reflections.

TABLE 8
Selected Interatomic Distances (Å) for (I) $Ba_2Nb_5O_9$, (II) $Ba_2Nb_{4.5(1)}Zr_{0.5(1)}O_9$, (III) $Ba_{3+\delta}Nb_{4.8(2)-\delta}Zr_{1.2(2)}O_{12-\delta}$, and (IV) $Ba_{4+\delta}Nb_{5.1(4)-\delta}Zr_{19(4)}O_{15-\delta}$

Bonding	(I)	Mult.	(II)	Mult.	(III)	Mult.	(IV)	Mult.
Ba1–O2	2.852(4)	×4	2.851(3)	×4	2.868(2)	×4	2.849(5)	×4
Ba1–O3	2.952(1)	×4	2.9551(2)	×4	2.9550(2)	×4	2.953(1)	×4
Ba1–O4	2.928(1)	×4	2.9410(4)	×4	2.987(3)	×4	2.986(5)	×4
Ba2–O4					2.923(3)	×8	2.912(5)	×4
Ba2–O5					2.9535(1)	×4	2.952(1)	×4
Ba2–O6							2.946(1)	×4
Nb1–Nb1	2.950(1)	×4	2.9534	×4	2.9535(1)	×4	2.952(1)	×4
Nb1–Nb2	2.890(1)	×4	2.8925(5)	×4	2.8969(5)	×4	2.898(1)	×4
Nb1–O1	2.086(1)	×2	2.0884(1)	×2	2.0884(1)	×2	2.087(1)	×2
Nb1–O2	2.113(6)	×2	2.123(4)	×2	2.100(4)	×2	2.126(7)	×2
Nb2–O2	2.089(1)	×4	2.0919(2)	×4	2.0905(2)	×4	2.090(1)	×4
Nb2–O3	2.161(9)		2.162(6)		2.152(5)		2.13(1)	
Nb3–O3	1.951(9)	×2	1.971(6)	×2	2.002(5)		2.02(1)	
Nb3–O4	2.086(1)	×4	2.0884(1)	×4	2.0888(1)	×4	2.087(1)	×4
Nb3–O5					2.0847(7)		2.08(1)	
Nb4–O5							2.08(1)	×2
Nb4–O6							2.0873	×4

Structural Aspects

The structure of the different homologues in the series nBaNbO$_3$ + 3mNbO can be described as an intergrowth of single NbO ($m = 1$) and multiple perovskite layers ($n = 2, 3, 4, 5$). In the NbO layer, Nb1 is planar four-coordinated by oxygen, as in pure NbO, while Nb2 is five-coordinated by a square pyramid. In the full perovskite unit (see Fig. 2), Nb atoms are octahedrally coordinated by six O atoms. A simple calculation using Pauling's electrostatic valence rule, with Ba set to 2+, yields a valence for Nb1 = + 2.11, Nb2 = + 2.89, and Nb3 (Nb3 and Nb4, depending on homologue) = + 4.0. This leads to 10 e^- being involved in metal–metal bonding in the NbO layer. Theoretical calculations predict 10–10.5 and observed values 9–11 electrons to be an optimum for stabilization of the NbO layer (2, 34). Assuming all perovskite metal positions to be occupied by Nb^{+5} yields $Ba_2Nb_5O_9$ having 11 e^- free for metal–metal bonding, $Ba_3Nb_6O_{12}$ having 12 e^-, and $Ba_4Nb_7O_{15}$ having 13 e^-. Thus, the replacement of Nb by Zr could theoretically be 100% in the perovskite, as this would yield 10 e^- in each case. However, assuming ~10.5 e^- to be needed for stabilization of the NbO layer yields $Ba_2Nb_{4.5}Zr_{0.5}O_9$, $Ba_3Nb_{4.5}Zr_{1.5}O_{12}$, and $Ba_4Nb_{5.5}Zr_{2.5}O_{15}$ as the extremes in Zr content for each homologue, respectively. These compositions are very close to those observed by EDS analysis and also to the refined compositions, thus supporting the above assumption. Considering the latter to be true, the average valence of Nb in the perovskite metal position for the homologues 2:1–5:1, containing no Zr, would be +4.5, +4.25, +4.17, and +4.13. With the cation content from the EDS analysis, and assuming the oxygen positions to be fully occupied ($\delta = 0$), the corresponding valences are +4.89, +5.00, +5.00, and +4.20. (The value + 4.20, for the 5:1 homologue, should not really be taken into consideration as the crystal is heavily disordered.) The values from EDS analysis also show that the system strives to replace as much of the Nb in the perovskite as allowed, keeping ~10.5 e^- in the NbO slab.

Ba–Ba interatomic distances parallel to the c-axis increase when Zr is introduced into $Ba_2Nb_5O_9$, see Table 9.

TABLE 9

Ba–Ba Distances (Å) Parallel to the *c* Axis for $Ba_2Nb_5O_9$, $Ba_2Nb_{4.5(1)}Zr_{0.5(1)}O_9$, $Ba_{3+\delta}Nb_{4.8(2)-\delta}Zr_{1.2(2)}O_{12-\delta}$, and $Ba_{4+\delta}Nb_{5.1(4)-\delta}Zr_{1.9(4)}$

Atoms	$Ba_2Nb_5O_9$	$Ba_2Nb_{4.5(1)}Zr_{0.5(1)}O_9$	$Ba_{3+\delta}Nb_{4.8(2)-\delta}Zr_{1.2(2)}O_{12-\delta}$	$Ba_{4+\delta}Nb_{5.1(4)-\delta}Zr_{1.9(4)}O_{15-\delta}$
Ba1–Ba1	4.110(6)	4.1416(7)		
Ba1–Ba2			4.1806(5)	4.166(2)
Ba2–Ba2				4.159(2)

TABLE 10

Bond-Order Sum Calculations for (I) $Ba_2Nb_5O_9$, (II) $Ba_2Nb_{4.5(1)}Zr_{0.5(1)}O_9$, (III) $Ba_{3+\delta}Nb_{4.8(2)-\delta}Zr_{12-\delta}O_{12-\delta}$ and (IV) $Ba_{4+\delta}Nb_{5.1(4)}Zr_{1.9(4)}O_{15-\delta}$ (Nb Replaced by Zr at i = Nb3, ii = Nb4, iii = Nb3 and Nb4)

Atom	$\sum s_i$ (I)	$\sum s_i$ (II)	$\sum s_i$ (III)	$\sum s_i$ (IV)
Ba1	2.23	2.23	2.12	2.14
Ba2			2.11	2.07
Nb1	2.40	2.37	2.42	2.34
Nb2	2.98	2.96	2.96	3.00
Nb3	4.29	4.18, 4.48[i]	3.91, 4.19[i]	3.86, 4.14[i, iii]
Nb4				3.75, 4.02[ii, iii]
O1	2.49	2.48	2.48	2.48
O2	2.25	2.23	2.25	2.22
O3	2.07	2.02, 2.08[i]	1.97, 2.03[i]	1.96, 2.01[i, iii]
O4	1.95	1.93, 2.02[i]	1.90, 1.99[i]	1.91, 2.00[i, iii]
O5			1.91, 2.00[i]	1.92, 1.97[i, ii]
O6				1.91, 2.00[ii, iii]

This indicates that the Ba1–O4 interaction is weakened, suggesting an increased valence of (Nb, Zr) in the $(Nb, Zr)O_6$ octahedra, which should be revealed as a shortening of the (Nb, Zr)–O3 distances. However, this effect seems to be overwhelmed by the replacement of Nb by the slightly larger Zr. The same phenomenon is found for the $n{:}m = 3{:}1$ homologue. In the 4:1 compound the Ba–Ba distance has decreased compared to that in the 3:1 homologue, but the trend of increasing Nb–O3 interatomic distance continues, although its e.s.d. is rather high.

A simple but surprisingly successful method for determining the valences of atoms in a crystal structure involves bond-order sum calculations (BOS), using the formula $v = \sum s = \exp((R_1 - R)/B)$ suggested by Brown and Altermatt (35) ($R_1(Ba^{2+}\text{–O}) = 2.285$ Å, $R_1(Nb^{5+}\text{–O}) = 1.911$ Å, $R_1(Zr^{4+}\text{–O}) = 1.937$ Å, $B = 0.37$). The results of the calculations are presented in Table 10. The v of the Ba atoms slightly exceeds the ideal value of $+2$, but this is in line with the results of the same calculations for similar compounds (1, 36). However, it is interesting to note that the v tends to decrease with increasing width of the perovskite layer. Comparing the results with $BaNbO_3$ (2.37) and $BaZrO_3$ (1.98) suggests that the decrease is due to an increased amount of Zr and the weakened Ba1–O4 interaction, as stated above. The BOS value for O1 (approx. 2.40) significantly deviates from those of the other oxygen atoms (O2–O6), but this is not unexpected, as a v of 2.41 is obtained for O1 from the same calculations for NbO. The seemingly high value is a direct result of using an R_1 value in the calculations that corresponds to Nb^{5+} and not to Nb^{2+}, which would be more appropriate. The remaining oxygen atoms show a span of v values between 1.90 and 2.25, fully in agreement with what is found in other reduced oxoniobates. The v values for Nb1, Nb2, and Nb3/Nb4 are all close to the values obtained by electrostatic calculations, and thus agree with expectation, although the values for Nb3/Nb4 indicate some kind of trend. A comparison of these values with the v for Nb and Zr calculated for $BaNbO_3$ (4.19) and $BaZrO_3$ (3.96), respectively, suggests that the decrease is a result of an increased amount of Zr, as one would expect. As stated above, the ideal number of free electrons for metal–metal bonding assigned to the NbO layer should be about 10–10.5. Calculating the corresponding number for each of the homologues (I–IV in Table 10) and $BaNb_4O_6$ (9.04) yields somewhat low values, between 9.04 and 9.34. These values show the limitations of using bond-order sums for calculating the number of valence electrons.

Zr Content Calculated Using Vegard's Law

Based on the structures of the different homologues, they can all be described as being formed by blocks of NbO, $BaNbO_3$, and $BaZrO_3$ (when Zr replaces Nb in the perovskite metal position). In this way, the c-axes of the different homologues (2:1, 3:1, 4:1, and 5:1) can be described as being one NbO block and $n = 2$, 3, 4, and 5 perovskite blocks long, respectively. The shortest c-axis will thus be obtained without any $BaNbO_3$ block replaced by $BaZrO_3$ ($x = 0$), and the longest with $n - x$ blocks replaced ($x = 1$, 2, 3, and 4 for each homologue, (respectively), assuming replacement of Nb only at the perovskite metal positions. The dilution of $BaNbO_3$ by $BaZrO_3$ in the different homologues can thus be said to follow the same linear behavior that Vegard's law presents for solid solutions (37). The best minimum $BaNbO_3$ block size to use for the calculation of the c-axis is probably that of $Ba_2Nb_5O_9$ (12.224/3 Å). Using Vegard's law, the c-axis can thus be calculated as $c = (n + m - x)(12.224/3) + x4.181$ Å, with x as above. The range of the c-axis length for each homologue would then be 12.224–12.330 Å for 2:1, 16.299–16.511 Å for 3:1, 20.373–20.692 Å for 4:1, and 24.448–24.873 Å for 5:1. With a reversed calculation, using the c-axis in each case (12.269 Å, 16.493 Å, 20.619 Å, and 24.804), Vegard's law yields $x = 0.42$, $x = 1.83$, $x = 2.30$, and $x = 3.35$ for each homologue, respectively. Notice that the first and third values are in good agreement with those found in the

structure refinements. However, it is more interesting to compare these values with those obtained from EDS analysis, which show a very good match for the 2:1, 3:1, and 4:1 homologues. The value for the 5:1 homologue deviates significantly from the value obtained in the EDS analysis, as expected for a severely disordered crystal.

CONCLUSION

The single-crystal investigation clearly shows that it is possible to replace some of the Nb in the structure by Zr. But it also shows that there are no indications of replacement of Nb in non-perovskite metal positions (the MO_6 octahedra). The behavior of Zr in these systems is completely in line with its reluctance to change oxidation state. The bond-order sum calculations and interatomic distance trends indicate that Nb must increase its valence in the perovskite in order to stabilize the structures. The expansion of the cell parameters is found to be directly proportional to the Zr content, thus obeying Vegard's law.

ACKNOWLEDGMENTS

We thank Professor Sven Lidin for valuable discussions, and the Swedish Natural Science Research Council for financial support.

REFERENCES

1. J. Köhler, G. Svensson, and A. Simon, *Angew. Chem., Int. Ed. Engl.* **31,** 1437 (1992).
2. G. Svensson, J. Köhler, and A. Simon, *in* "Metal Clusters in Chemistry" (P. Braustein, L. A. Oro, and R. R. Raithling, Eds.). Wiley-VCH, Weinheim, Germany, 1999.
3. B. O. Marinder, *Chem. Scr.* **11,** 97 (1977).
4. J. Köhler and A. Simon, *Z. Anorg. Allg. Chem.* **553,** 106 (1987).
5. K. B. Kersting and W. Jeitschko, *J. Solid State Chem.* **93,** 350 (1991).
6. J. Köhler, A. Simon, R. Tischtau, and G. Miller, *Angew. Chem., Int. Ed. Engl.* **28,** 1662 (1989).
7. G. Svensson and J. Grins, *Acta Crystallogr. B* **49,** 626 (1993).
8. V. G. Zubkov, V. A. Perelyaev, A. P. Tyutyunnik, I. A. Kontsevaya, O. V. Makarova, and A. G. P. Shveikin, *Sov. Phys. Dokl.* **37,** 386 (1992).
9. V. G. Zubkov, V. A. Perelyaev, A. P. Tyutyunnik, I. A. Kontsevaya, V. I. Vornin, and G. Svensson, *J. Alloys Compd.* **203,** 209 (1994).
10. G. Svensson, *Mater. Res. Bull.* **23,** 437 (1988).
11. G. Svensson, J. Köhler, and A. Simon, *J. Alloys Compd.* **176,** 123 (1991).
12. G. Brauer, *Z. Anorg. Allg. Chem.* **248,** 1 (1941).
13. H. Schäfer and H.-G. Schnering, *Angew. Chem.* **76,** 833 (1964).
14. G. Svensson, *Microsc. Microanal. Microstruct.* **1,** 343 (1990).
15. A. Magnéli, *Microsc. Microanal. Microstruct.* **1,** 1 (1990).
16. G. Svensson, *J. Solid State Chem.* **90,** 249 (1991).
17. G. Svensson, J. Köhler, and A. Simon, *Angew. Chem., Int. Ed. Engl.* **104,** 192 (1992).
18. G. Svensson and L. Eriksson, *J. Solid State Chem.* **114,** 301 (1995).
19. G. Svensson, L. Eriksson, C. Olofsson, and W. Holm, *J. Alloys Compd.* **248,** 33 (1997).
20. D. Watanabe, J. R. Castles, A. Jotsons, and A. S. Malin, *Acta Crystallogr.* **23,** 307 (1967).
21. D. Watanabe, O. Terasaki, A. Jotsons, and J. R. Castles, *J. Phys. Soc. Jpn.* **25,** 292 (1968).
22. V. R. Scholder, D. Räde, and H. Schwarz, *Z. Anorg. Allg. Chem.* **362,** 149 (1968).
23. A. L. Bowman, T. C. Wallece, J. L. Yarnell, and R. G. Wenzel, *Acta Crystallogr.* **21,** 843 (1966).
24. M. T. Casais, J. A. Alonso, I. Rasines, and M. A. Hidalgo, *Mater. Res. Bull.* **30,** 201 (1995).
25. V. A. Perelyaev, L. D. Miroshnikova, S. I. Alyamovskii, and D. G. Kellerman, *Russ. J. Inorg. Chem.* (*Engl. Trans.*) **34,** 418 (1989).
26. B. Bondars, G. Heidemane, J. Grabis, K. Laschke, H. Boysen, J. Schneider, and F. Frey, *J. Mater. Sci.* **30,** 1621 (1995).
27. G. Nilsson and G. Svensson, submitted to *J. Alloys Compd.* (2000).
28. K. E. Johansson, T. Palm, and P. E. Werner, *J. Phys. E* **13,** 1289 (1980).
29. Stoe, *Stoe IPDS*, Software manual ver. 2.87, 1987.
30. V. Petricek and M. Dusek, *Jana98*, 1997.
31. C. E. Michelson, P. E. Rauch, and F. J. DiSalvo, *Mater. Res. Bull.* **25,** 971 (1990).
32. V. G. Zubkov, V. A. Pereleyaev, D. G. Kellermann, V. E. Stpsev, V. P. Dyakina, I. A. Kontsevaya, O. B. Makrova, and G. P. Shveikin, *Dokl. Akad. Nauk., SSSR* **313,** 367 (1990).
33. C. Giacovazzo, H. L. Monaco, D. Viterbo, F. Scordari, G. Gilli, G. Zanotti, and M. Catti, *in* "Fundamentals of Crystallography—2" (C. Giacovazzo, Ed.), Second Edition, p. 164. The Bath Press, Avon, 1992.
34. G. V. Vajenine and A. Simon, *Inorg. Chem.* **38,** 3463 (1999).
35. I. D. Brown and D. Altermatt, *Acta Crystallogr. B* **41,** 244 (1985).
36. G. Nilsson and G. Svensson, *Z. Anorg. Allg. Chem.* **626,** 160 (2000).
37. A. R. West, "Solid State Chemistry and its applications." Wiley, New York, 1984.